Burtt, D.G., et al., 2022, Hot atmospheric formation of carbonate accretionary lapilli at the Cretaceous-Paleogene boundary, Brazos River, Texas, from clumped isotope thermometry: Geology, v. 50, https://doi.org/10.1130/G49674.1

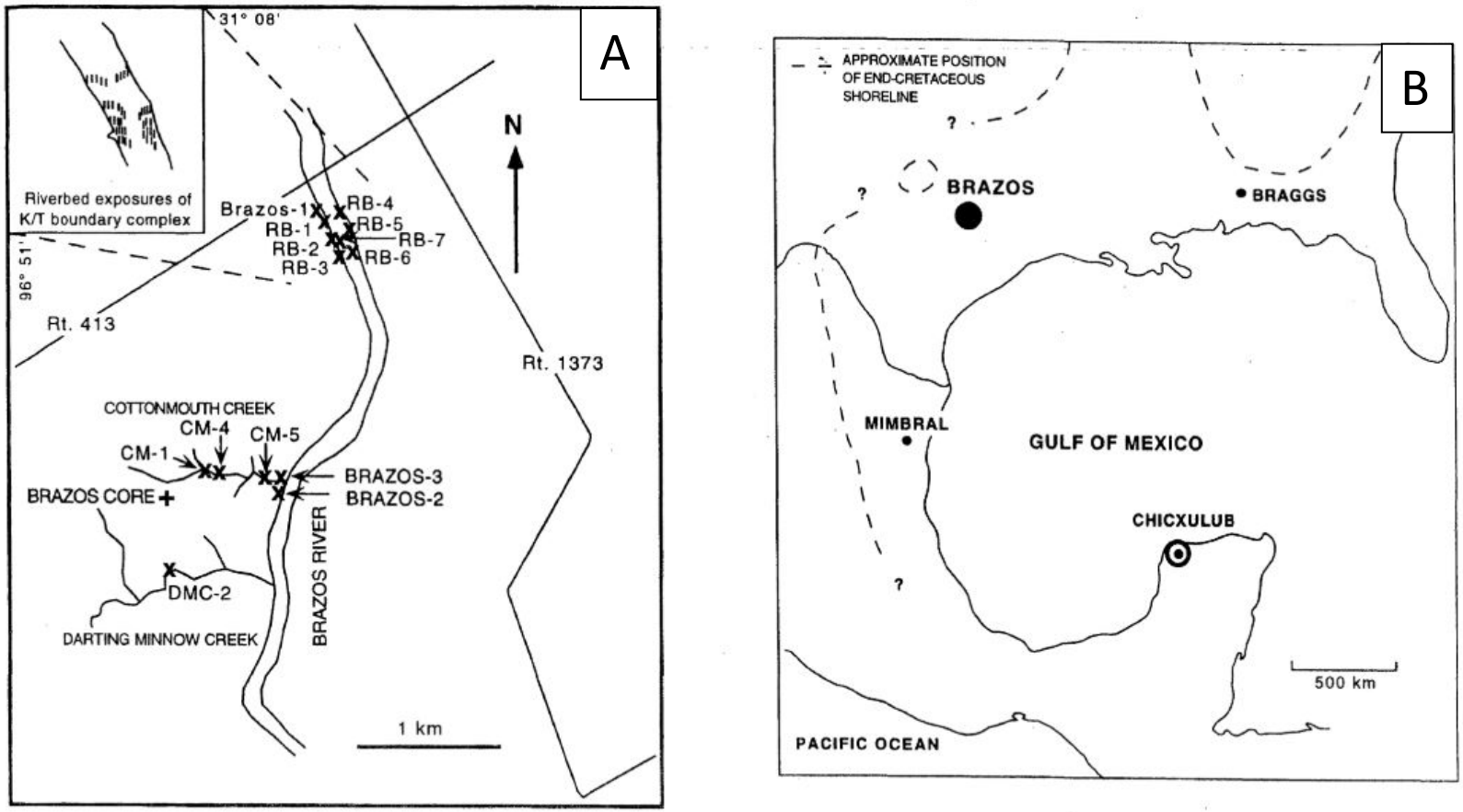

Figure S1 (adapted from Yancey, 1996): Maps showing (A) the locations of the sampled 'RB' sections along the Brazos River channel (these have since eroded away), relative to other outcrops and the Brazos sediment core, and (B) a comparison of the Brazos River locality to other, select K-Pg boundary sites surrounding the Gulf of Mexico. All samples were collected by Yancey and colleagues and the remaining samples are stored at Stony Brook University.

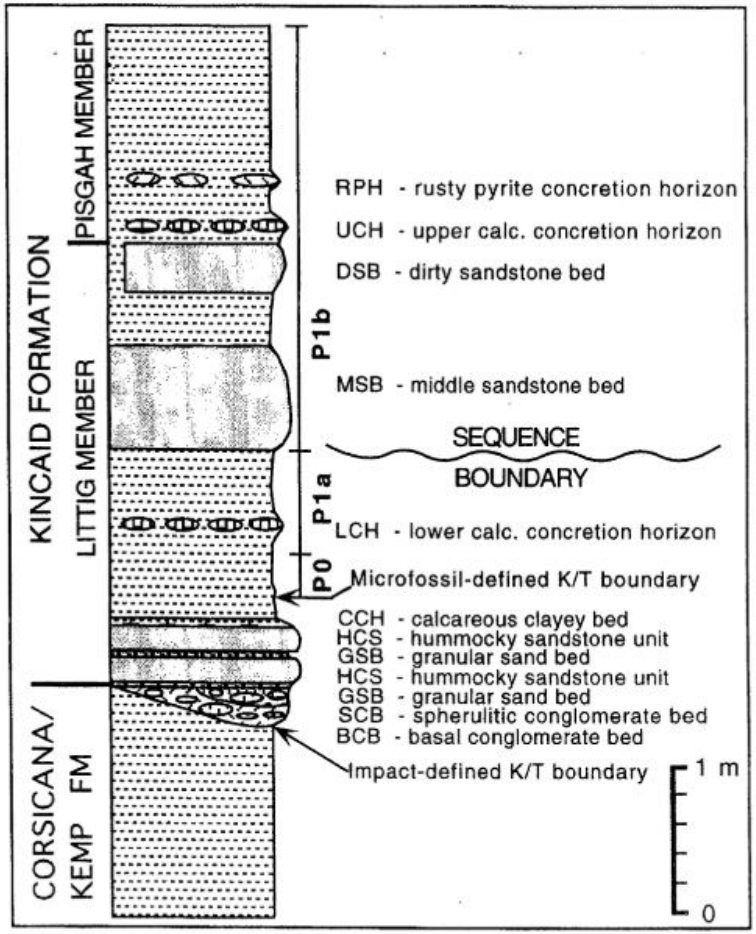

Figure S2 (adapted from Yancey, 1996): A composite stratigraphic column of the K-Pg boundary sequence at the Brazos River, TX. This column includes planktic foraminifera zones (P0, P1a, and P1b) as identified by Keller (1989) and Hansen et al. (1993), as well as the impact-defined and microfossil-defined K-Pg boundaries. Lapilli, foraminifera, and mudstone samples were all taken from the sections in between these boundary layers. Iridium anomalies are documented at the top of the CCH bed and at the microfossil-defined boundary (Yancey, 1996).

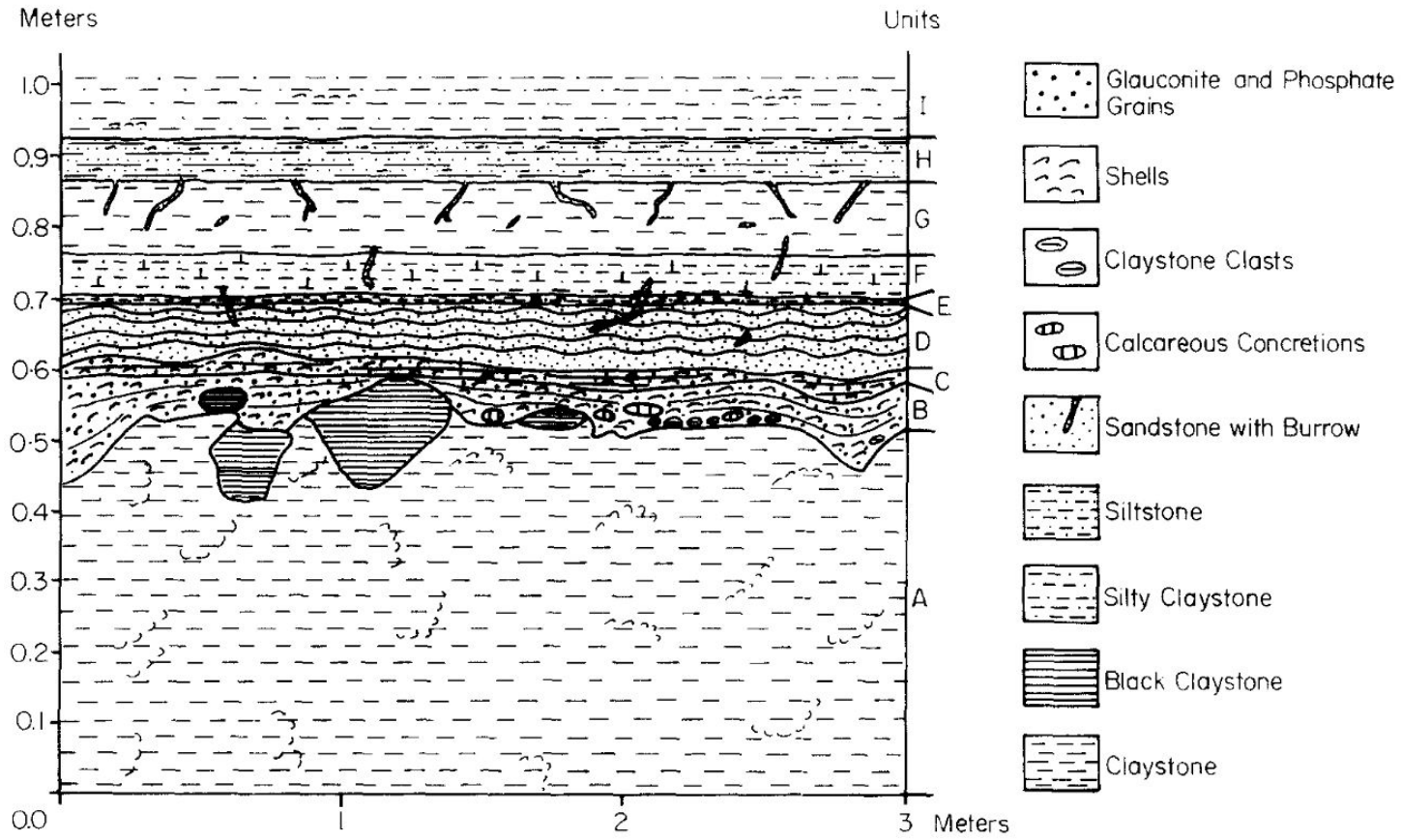

Figure S3 (adapted from Hansen et al., 1987): A representative stratigraphic section from the Brazos-1 outcrop along the Brazos River, TX (shown geographically in Fig. S1). Unit A corresponds to the late Cretaceous Corsicana Formation while Unit I corresponds to the clay-rich component of the the Kincaid Formation, both of which can be seen in Fig. S2. Units B through H therefore correspond to the K-Pg boundary units referenced in Yancey (1996). While there are similarities in between this figure and Fig. S2, it is stressed that this figure is based on the Brazos-1 section while Fig. S2 is based on the RB sections where the samples in this study were collected (Fig. S1).

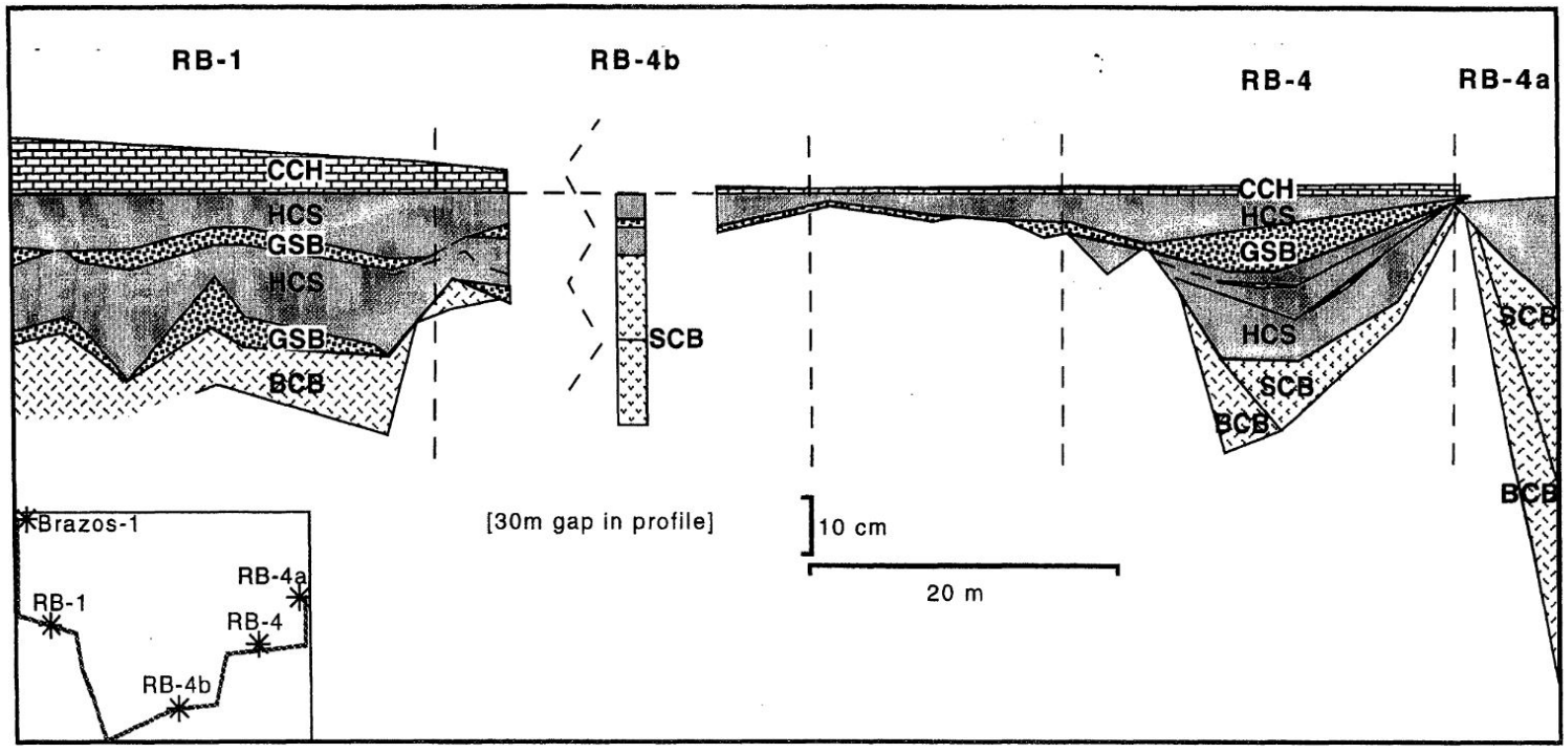

Figure S4 (from Yancey, 1996): Cross sectional view of the Brazos River K-Pg boundary sections going from western river bank (RB-1) to the eastern river bank (RB-4). Lapilli isotope data are from both RB-1 and RB-4a. The unit nomenclature is the same as that established in Figure S2. Vertical dashed lines denote a change in profile, which can also be seen in the inset. The jagged dashed line marks a 30 m gap between outcrops. The zero datum line is set at the contact between the CCH layer and the HCS bed. The SCB bed of RB-4b is split in two based on the relative amount of spherules in the two parts of the unit (higher concentration in the upper part).

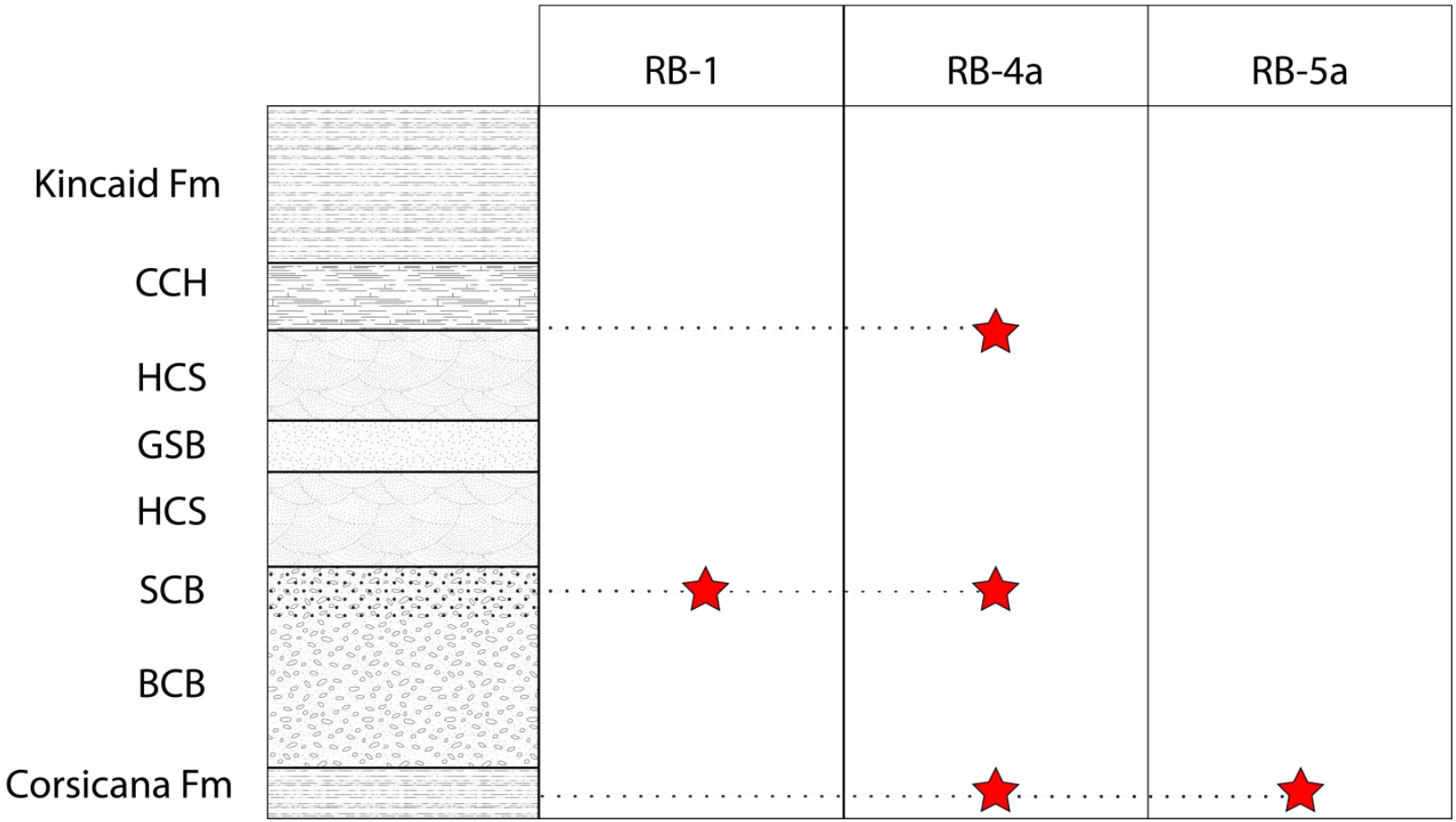

Figure S5: Carbonate lapilli relationships to stratigraphy at the K-Pg boundary, Brazos River, TX. The unit names follow the nomenclature in Figure S2. The red stars indicate where lapilli were collected for stable isotope analysis. The top star is RB-4a-50cmb-2, the middle stars are RB-1-SCBbed-4 and RB-4a-SCBbed-3, and the lower stars are RB-4a-1 and RB-5a-5. The thickness of the units is not to scale as many beds are not laterally continuous between the measured sections (Fig. S4. The placement of stars shows the relative position of samples to each other across sections (seen in Fig. S1A) More detailed stratigraphy can be found in Yancey (1996).

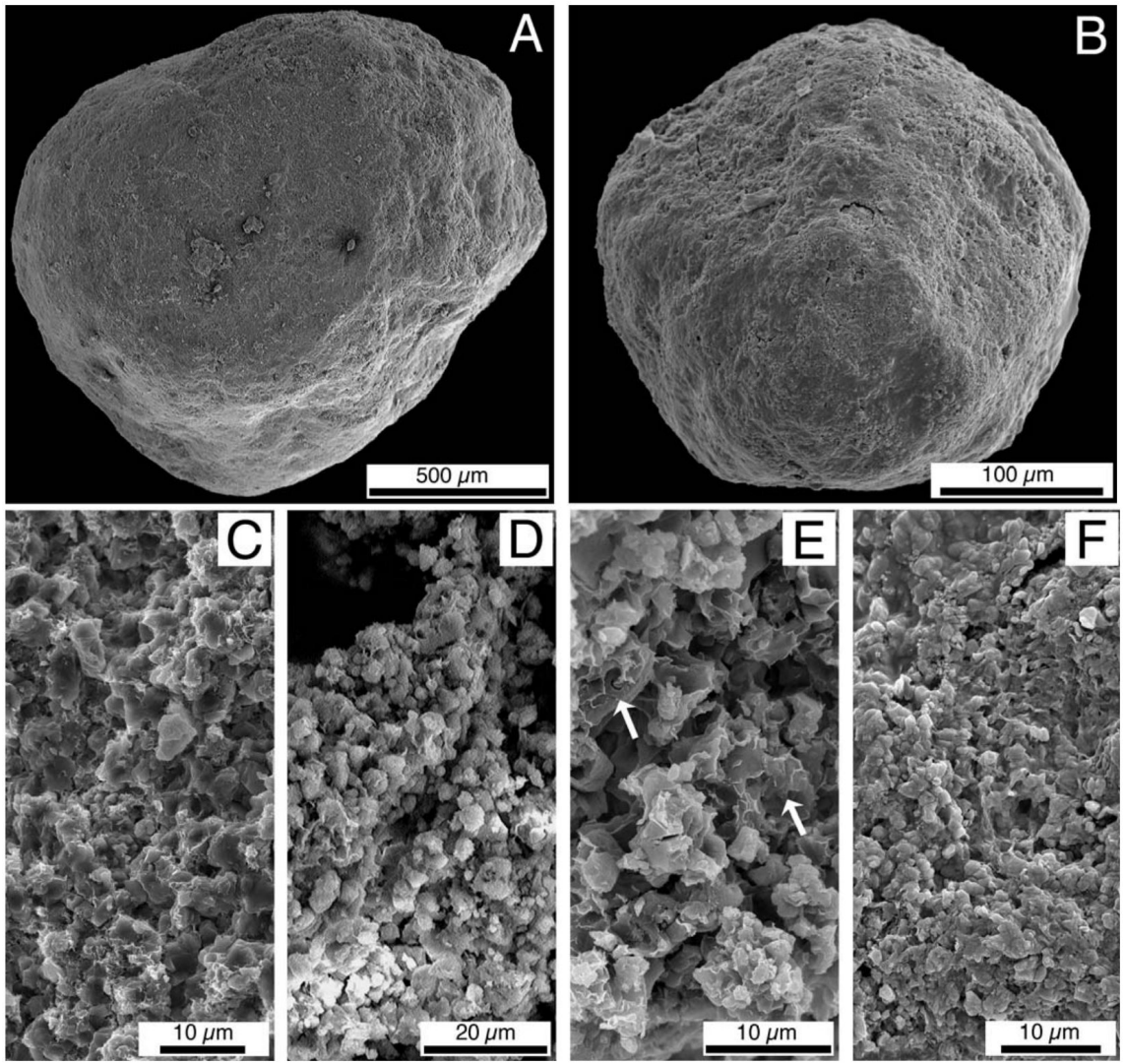
A
500 μm
B
100 μm
C
10 μm
D
20 μm
E
10 μm
F
10 μm

reinforcing the primary interpretation, and are generally consistent with the morphology of samples selected for isotope analysis in this study. Further discussion of these SEM images can be found in Yancey & Guillemette (2008).

Table S1. CARBON, OXYGEN, AND CLUMPED ISOTOPE RESULTS FOR ACCRETIONARY LAPILLI, FORAMINIFERA, AND A CARBONATE-RICH MUDSTONE

Sample ID	Place of Analysis*	# of Lapilli/Forams**	Size (mm)	n	$\delta^{13}C$ (‰, VPDB)	$\delta^{18}O$ (‰, VPDB)	Δ_{47} (‰, CDES @ 90 °C)	$T(\Delta_{47})$ (°C)$^{\$}$	$\delta^{18}O_w$ (‰, SMOW)$^{\$\$}$
Lapilli									
RB-4a-SCBed-#3-1	JHU	1	2.0	1	-9.73	-4.07	0.558	39	0.6
RB-4a-SCBed-#3-2	JHU	6	1.0	1	-8.25	-4.41	0.530	50	2.1
RB-4a-SCBed-#3-3	HU	1	N.D.	1	-7.27	-5.03	0.436	96	7.7
RB-4a-SCBed-#3-4	HU	1	N.D.	1	-6.10	-5.72	0.455	85	5.7
RB-4a-SCBed-#3-5	HU	1	N.D.	1	-9.28	-4.21	0.445	90	7.9
RB-4a-SCBed-#3-6	SBU	9	1.0	1	-8.89	-4.43	0.491	67	4.7
RB-4a-SCBed-#3-7	SBU	4	1.4	1	-7.53	-4.77	0.423	104	8.8
RB-4a-SCBed-#3-8	SBU	5	1.3	1	-9.22	-4.07	0.436	96	8.7
RB-4a-SCBed-#3-9	SBU	6	1.2	1	-8.92	-4.31	0.459	83	6.9
RB-4a-SCBed-#3-10	SBU	8	1.0	1	-6.89	-4.62	0.424	103	8.9
RB-4a-SCBed-#3-11	SBU	4	1.2	1	-9.42	-3.65	0.491	67	5.5
RB-4a-SCBed-#3-12	SBU	11	0.9	1	-8.88	-4.23	0.448	89	7.7
RB-4a-SCBed-#3 *Avg.*				*12*	*-8.37*	*-4.46*	*0.466*	*79*	*6.3*
1σ Standard Deviation					*1.15*	*0.53*	*0.012 (SE)*	*7 (SE)*	*0.8*
RB-4a-50cmb-#2-1	JHU	1	2.5	1	-5.00	-6.64	0.501	62	1.8
RB-4a-50cmb-#2-2	JHU	5	1.5	1	-4.41	-5.81	0.412	111	8.5
RB-4a-50cmb-#2-3	HU	1	N.D.	1	-7.38	-6.53	0.352	159	11.8
RB-4a-50cmb-#2-4	HU	1	N.D.	1	-4.90	-6.85	0.258	293	17.8
RB-4a-50cmb-#2-5	HU	1	N.D.	1	-5.14	-7.18	0.293	229	15.0
RB-4a-50cmb-#2-6	HU	1	N.D.	1	-7.39	-6.41	0.228	370	20.2
RB-4a-50cmb-#2-7	SBU	1	2.2	1	-5.43	-6.69	0.340	171	12.4
RB-4a-50cmb-#2-8	SBU	1	2.5	1	-5.82	-6.87	0.381	134	9.5

RB-4a-50cmb-#2-9	SBU	1	2.5	1	-6.13	-6.94	0.418	107	7.0
RB-4a-50cmb-#2-10	SBU	2	2.3	1	-6.66	-6.73	0.378	136	9.9
RB-4a-50cmb-#2-11	SBU	2	2.0	1	-4.89	-6.83	0.409	113	7.7
RB-4a-50cmb-#2-12	SBU	2	1.8	1	-5.90	-6.64	0.381	134	9.7
RB-4a-50cmb-#2-13	SBU	1	2.8	1	-5.36	-7.28	0.344	167	11.6
RB-4a-50cmb-#2 *Avg.*				*13*	*-5.72*	*-6.72*	*0.361*	*151*	*11.0*
1σ Standard Deviation					*0.95*	*0.37*	*0.020 (SE)*	*18 (SE)*	*1.3*
RB-5a-#5-1	JHU	4	1.5	1	-5.05	-7.24	0.455	85	4.2
RB-5a-#5-2	JHU	1	2.5	1	-3.85	-5.36	0.426	102	8.0
RB-5a-#5-3	HU	1	N.D.	1	-5.28	-6.59	0.499	63	1.9
RB-5a-#5-4	HU	1	N.D.	1	-5.50	-6.81	0.503	62	1.5
RB-5a-#5-5	HU	1	N.D.	1	-4.53	-6.74	0.493	66	2.2
RB-5a-#5-6	HU	1	N.D.	1	-4.03	-7.03	0.436	96	5.7
RB-5a-#5-7	SBU	1	1.7	1	-5.38	-6.40	0.419	107	7.5
RB-5a-#5-8	SBU	1	2.5	1	-3.76	-6.97	0.384	132	9.2
RB-5a-#5-9	SBU	2	1.9	1	-5.81	-6.83	0.463	81	4.1
RB-5a-#5-10	SBU	5	1.4	1	-5.59	-6.45	0.398	121	8.8
RB-5a-#5-11	SBU	2	1.8	1	-5.64	-6.39	0.459	83	4.8
RB-5a-#5-12	SBU	2	1.6	1	-5.67	-6.73	0.393	125	8.8
RB-5a-#5-13	SBU	4	1.8	1	-5.90	-6.64	0.381	134	9.7
RB-5a-#5-14	SBU	2	2.8	1	-5.36	-7.28	0.344	167	11.6
RB-5a-#5 *Avg.*				*14*	*-5.10*	*-6.68*	*0.432*	*98*	*6.3*
1σ Standard Deviation					*0.74*	*0.47*	*0.013 (SE)*	*8 (SE)*	*0.9*
RB-1-SCBbed-#4-1	JHU	20	1	1	-2.37	-7.39	0.368	145	9.8
RB-1-SCBbed-#4-2	JHU	5	1.5	1	-3.32	-7.12	0.401	119	7.9
RB-1-SCBbed-#4-3	HU	1	N.D.	1	-2.10	-7.72	0.446	90	4.3
RB-1-SCBbed-#4-4	SBU	13	0.9	1	-2.25	-7.61	0.370	143	9.5
RB-5a-#5 *Avg.*				*4*	*-2.51*	*-7.46*	*0.396*	*122*	*7.9*

1σ Standard Deviation					*0.55*	*0.27*	*0.018*	*13*	*1.3*
RB-4a-#1-1	JHU	1	2.5	1	-7.13	-6.91	0.391	126	8.8
RB-4a-#1-2	JHU	5	1.5	1	-5.91	-6.92	0.334	177	12.6
RB-4a-#1-3	HU	1	N.D.	1	-9.38	-5.91	0.360	152	11.9
RB-4a-#1-4	HU	1	N.D.	1	-8.92	-6.10	0.444	92	6.1
RB-4a-#1-5	HU	1	N.D.	1	-8.18	-6.59	0.355	156	11.5
RB-4a-#1-6	HU	1	N.D.	1	-8.07	-6.31	0.393	124	9.3
RB-4a-#1-7	SBU	1	2.3	1	-6.85	-6.79	0.367	145	10.5
RB-4a-#1-8	SBU	1	2.6	1	-6.22	-7.14	0.416	109	6.9
RB-4a-#1-9	SBU	1	2.6	1	-7.44	-7.03	0.437	95	5.6
RB-4a-#1-10	SBU	1	3.5	1	-5.34	-6.97	0.412	111	7.3
RB-4a-#1-11	SBU	4	1.8	1	-7.33	-6.58	0.376	137	10.1
RB-4a-#1-12	SBU	1	2.9	1	-7.83	-6.36	0.410	113	8.1
RB-4a-#1-13	SBU	2	1.8	1	-6.72	-6.79	0.337	175	12.5
RB-4a-#1-14	SBU	2	2.3	1	-7.14	-6.53	0.365	147	10.9
RB-4a-#1-15	SBU	3	1.8	1	-6.94	-6.73	0.382	133	9.6
RB-4a-#1 *Avg.*				*15*	*-7.29*	*-6.64*	*0.385*	*130*	*9.4*
1σ Standard Deviation					*1.08*	*0.35*	*0.009*	*7*	*0.6*
Foraminifera									
top-Cret-Ln-1	HU	N.D.	N.D.	1	0.342	-1.364	0.680	26	0.6
top-Cret-Ln-2	HU	N.D.	N.D.	1	0.461	-1.320	0.701	19	-0.7
top-Cret-Ln-3	HU	N.D.	N.D.	1	0.198	-1.513	0.679	26	0.5
top-Cret-Ln-4	HU	N.D.	N.D.	1	0.183	-1.468	0.678	26	0.7
top-Cret-Ln *Avg.*				*4*	*0.30*	*-1.42*	*0.685*	*24*	*0.3*
1σ Standard Deviation					*0.07*	*0.04*	*0.005*	*2*	*0.3*
RB4a-BcB-bed-Ln-1	HU	N.D.	N.D.	1	-0.01	-1.66	0.668	29	1.1
RB4a-BcB-bed-Ln-2	HU	N.D.	N.D.	1	0.77	-1.94	0.706	18	-1.7

RB4a-BcB-bed-Ln-3	HU	N.D.	N.D.	1	0.32	-1.74	0.687	23	-0.2
RB4a-BcB-bed-Ln-4	HU	N.D.	N.D.	1	-0.29	-2.69	0.748	6	-5.2
RB4a-BcB-bed-Ln-5	HU	N.D.	N.D.	1	-0.51	-2.37	0.719	14	-3.0
RB4a-BcB-bed-Ln *Avg.*				*5*	*0.06*	*-2.08*	*0.706*	*18*	*-1.8*
1σ Standard Deviation					*0.23*	*0.20*	*0.014*	*4*	*1.1*
CMC#1-1	SBU	20	1.0	1	0.26	-1.68	0.658	37	2.5
CMC#1-2	SBU	20	1.0	1	0.18	-1.67	0.650	39	3.0
CMC#1-3	SBU	21	1.0	1	0.09	-1.66	0.663	35	2.2
CMC#1 *Avg.*				*3*	*0.18*	*-1.67*	*0.657*	*37*	*2.6*
1σ Standard Deviation					*0.05*	*0.00*	*0.004*	*1*	*0.2*
CMC#2-1	SBU	13	1.2	1	0.16	-1.41	0.671	32	1.7
CMC#2-2	SBU	22	1.1	1	0.15	-1.27	0.683	28	1.0
CMC#2-3	SBU	23	0.8	1	-0.09	-1.53	0.639	43	3.8
CMC#2 *Avg.*				*3*	*0.19*	*-1.55*	*0.665*	*35*	*2.2*
1σ Standard Deviation					*0.06*	*0.03*	*0.013*	*5*	*0.9*
CMC#4-1	SBU	20	1.0	1	0.29	-1.59	0.682	29	1.2
CMC#4-2	SBU	20	1.1	1	0.08	-1.49	0.667	34	2.3
CMC#4-3	SBU	21	0.9	1	0.20	-1.56	0.655	38	2.8
CMC#4 *Avg.*				*3*	*0.07*	*-1.40*	*0.674*	*33*	*2.1*
1σ Standard Deviation					*0.08*	*0.08*	*0.007*	*3*	*0.5*
Carbonate-rich Mudstone									
CCH-mud-1	HU	N.D.	N.D.	1	-9.32	-2.85	0.663	31	0.2
CCH-mud-2	HU	N.D.	N.D.	1	-9.31	-2.98	0.691	22	-1.7
CCH-mud-3	HU	N.D.	N.D.	1	-9.26	-3.02	0.720	14	-3.7
CCH-mud-4	HU	N.D.	N.D.	1	-9.35	-2.96	0.708	17	-2.8
CCH-mud-5	HU	N.D.	N.D.	1	-9.38	-2.87	0.687	23	-1.3

CCH-mud-6	HU	N.D.	N.D.	1	-9.35	-2.94	0.642	38	1.5
CCH-mud-7	HU	N.D.	N.D.	1	-9.31	-2.98	0.639	40	1.7
CCH-mud-8	HU	N.D.	N.D.	1	-9.37	-2.89	0.687	23	-1.4
CCH-mud-9	SBU	N.D.	N.D.	1	-9.41	-2.94	0.680	29	-0.3
CCH-mud-10	SBU	N.D.	N.D.	1	-9.43	-3.00	0.657	37	1.2
CCH-mud-11	SBU	N.D.	N.D.	1	-9.49	-2.87	0.650	40	1.9
CCH-Mud *Avg.*				*11*	*-9.36*	*-2.94*	*0.675*	*29*	*-0.4*
1σ Standard Deviation					*0.02*	*0.02*	*0.008*	*3*	*0.6*

Notes: *JHU = Johns Hopkins University, HU = Harvard University, SBU = Stony Brook University

**Denotes the number of lapilli or foraminifera tests that were homogenized for that analysis.
$T($\Delta_{47}$) calculated using Equation 1 from Petersen et al (2019). This study shares nearly identical analytical methods to those used here and the calibration is for the 25-350 °C temperature range.
$$Water oxygen isotope ratios calculated using T(Δ_{47}) and the calcite-water equilibrium fractionation from O'Neil et al (1969). All foraminifera analyzed were calcitic.

Table S2: CARBON, OXYGEN, AND CLUMPED ISOTOPE RESULTS FROM CARBONATE STANDARDS MEASURED AT JOHNS HOPKINS (JHU), HARVARD (HU), AND STONY BROOK (SBU)

ID	n	$\delta^{13}C$ corr (‰, VPDB)	$\delta^{13}C$ SD	$\delta^{18}O$ corr (‰, VPDB)	$\delta^{18}O$ SD	Δ_{47} (‰,, CDES90)	Δ_{47} SE
In house Carrara							
SBU	8	2.08	0.20	-1.87	0.27	0.301	0.010
JHU	13	2.33	0.01	-1.83	0.05	0.305	0.017
HU	31	2.29	0.02	-1.77	0.06	0.314	0.004
IAEA-603/NBS-19							
IAEA-603 (SBU)	14	2.46	0.13	-2.37	0.09	0.283	0.004
NBS-19 (JHU)	3	2.00	0.03	-2.23	0.03	0.326	0.006
NBS-18							
SBU	6	-5.01	0.03	-23.24	0.15	0.384	0.005
HU	3	-4.96	0.01	-23.16	0.03	0.374	0.002
HC-1							
SBU	9	-4.94	0.16	-6.96	0.12	0.540	0.005

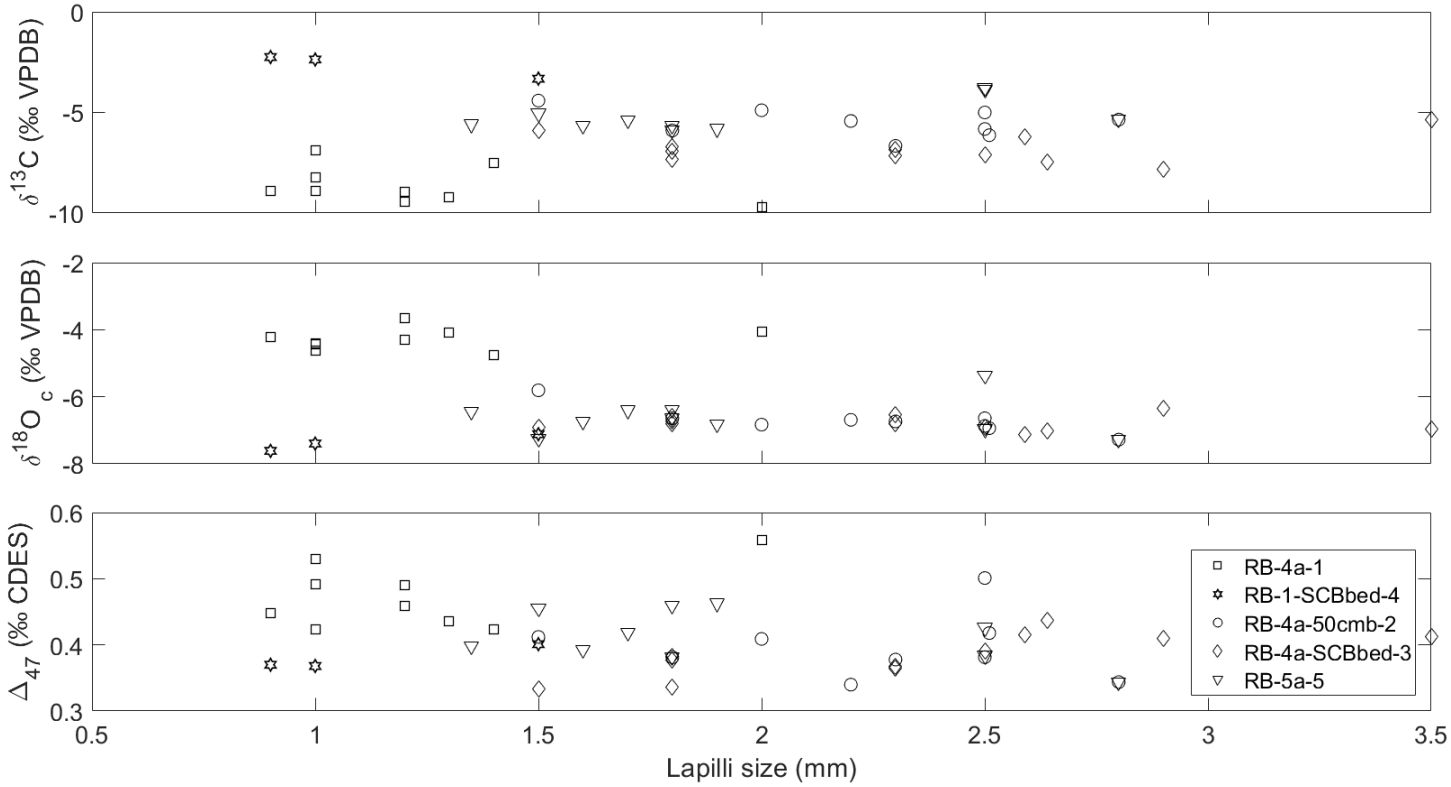

Figure S6: Lapilli size (mm) plotted against the three isotope systems (carbon, oxygen, and clumped). The lack of correlation rules out the possibility that grain size is responsible for the isotopic trends discussed in the main text.

Section S1. Rayleigh fractionation curves

Our model in Figure 3 uses two equations, the first for batch fractionation and the second for Rayleigh fractionation:

$$\delta^{13}C_f = \delta^{13}C_o - ((1 - F_C) * 1000 * \ln(\alpha)) \quad \text{(S1)}$$

$$\delta^{13}C_f = 1000 * (F_C^{\alpha-1} - 1) + \delta^{13}C_o \quad \text{(S2)}$$

In both equations, α is the equilibrium fractionation factor between CO_2 and $CaCO_3$ and F is the extent of reaction (F = 1 implies no reaction while F = 0 implies the reaction has gone to completion). These same equations can be used to calculate $\delta^{18}O$ by swapping out for the corresponding δ, α, and F values for oxygen.

To contextualize the measured lapilli $\delta^{13}C$ and $\delta^{18}O$ values we used a $^{13}\alpha$ of 1.0029363 and an $^{18}\alpha$ 1.0033055, based on the regressions of Scheele & Hoefs (1992) and Rosenbaum (1994), respectively. We selected that particular α value for oxygen from Scheele & Hoefs (1992) as their 900 °C experiments were conducted at 1 kbar, which we believe most closely approximates the conditions in the impact plume rather than using the higher T experiments performed at higher pressures. The initial, impacted carbonate rock $\delta^{13}C$ and $\delta^{18}O$ values, 1.5‰ and -1.5‰ respectively, were chosen based on measurements of a late Cretaceous shelf carbonate but are more generally representative of shelf carbonates from the late Mesozoic (Fouke et al., 2002). The initial isotope and α values for carbon and oxygen isotopes are constants in Eqns. S1 and S2, but F can vary between 1 and 0 as decarbonation progresses (Baumgartner & Valley, 2001). Because the carbon lost in $CaCO_3$ decomposition becomes CO_2, $\delta^{13}C$ changes as a function of F_C from 1 all the way to 0 (whereby all $CaCO_3$ is CO_2). F_O, on the other hand, will vary depending on the amount of oxygen-bearing species present (*e.g.* water, silicates, etc.). For example, as demonstrated by Baumgartner & Valley (2001), there is a so-called "calc-silicate limit" at F_O = 0.6 as the presence of silicates inhibits the transformation of oxygen from the carbonate phase into CO_2. With lower amounts of silicates, F_O can approach 0.3 where two-thirds of the oxygen are going to CO_2 and one-third remains as CaO. However, as seen in Fig. 3 in the main text, the Rayleigh fractionation appears to only capture the Chicxulub lapilli $\delta^{13}C$ and $\delta^{18}O$ data when F_O is between ~0.2 and 0. This implies a partial or complete disequilibrium between decarbonate and any associated silicate or oxide. The lapilli isotope data, which we hypothesize to have yielded from this style of isotope fractionation, are nominally similar to extreme ^{13}C and ^{18}O depletion trends associated with contact metamorphism (e.g., Table 1 in Baumgartner & Valley, 2001).

References:

Baumgartner, L.P., & Valley, J.W., 2001, Stable isotope transport and contact metamorphic fluid flow: Reviews in Mineralogy and Geochemistry, v. 43(1), p. 415-467.

Fouke, B.W., Zerkle, A.L., Alvarez, W., Pope, K.O., Ocampo, A.C., Wachtman, R.J., Nishimura, J.M.G., Claeys, P., and Fischer, A.G., 2002, Cathodoluminescence petrography and isotope geochemistry of KT impact ejecta deposited 360 km from the Chicxulub crater, at Albion island, Belize: Sedimentology, v. 49, p. 117–138, doi:10.1046/j.1365-3091.2002.00435.x.

Hansen, T., Farrand, R.B., Montgomery, H.A., Billman, H.G., and Blechschmidt, G., 1987, Sedimentology and extinction patterns across the Cretaceous-Tertiary boundary interval in east Texas: Cretaceous Research, v. 8, p. 229–252, doi:10.1016/0195-6671(87)90023-1.

Hansen, T.A., Upshaw III, B., Kauffman, E.G. and Gose, W., 1993. Patterns of molluscan extinction and recovery across the Cretaceous-Tertiary boundary in east Texas; report on new outcrops. *Cretaceous Research*, *14*(6), pp.685-706.

Keller, G., Abramovich, S., Berner, Z., and Adatte, T., 2009, Biotic effects of the Chicxulub impact, K-T catastrophe and sea level change in Texas: Palaeogeography, Palaeoclimatology, Palaeoecology, v. 271, p. 52–68, doi:10.1016/j.palaeo.2008.09.007.

O'Neil, J.R., Clayton, R.N., and Mayeda, T.K., 1969, Oxygen isotope fractionation in divalent metal carbonates: The Journal of Chemical Physics, v. 51, p. 5547–5558, doi:10.1063/1.1671982.

Rosenbaum, J. M., 1994, Stable isotope fractionation between carbon dioxide and calcite at 900 C: Geochimica et Cosmochimica Acta, v. 58(17), p. 3747-3753.

Scheele, N., & Hoefs, J., 1992, Carbon isotope fractionation between calcite, graphite, and CO2: an experimental study: Contributions to Mineralogy and Petrology, v. 112(1), p. 35-45.

Yancey, T.E., 1996, Stratigraphy and Depositional Environments of the Cretaceous-Tertiary Boundary Complex and Basal Paleocene Section, Brazos River, Texas: Transactions of the Gulf Coast Association of Geological Societies, v. 80, p. 433–442, doi:10.1306/64ed9e3e-1724-11d7-8645000102c1865d.

Yancey, T.E., and Guillemette, R.N., 2008, Carbonate accretionary lapilli in distal deposits of the Chicxulub impact event: Bulletin of the Geological Society of America, v. 120, p. 1105–1118, doi:10.1130/B26146.1.